

Two-Order Targeted Brain Tumor Imaging By Using An Optical/ Paramagnetic Nanoprobe across the Blood Brain Barrier

Huihui Yan, Lu Wang, Jiyao Wang, Xiaofu Weng, Hao Lei, Xuxia Wang, Lu Jiang, Jianhua Zhu, Weiyue Lu, Xunbin Wei, and Cong Li

ACS Nano, **Just Accepted Manuscript** • Publication Date (Web): 11 Dec 2011

Downloaded from <http://pubs.acs.org> on December 19, 2011

Just Accepted

“Just Accepted” manuscripts have been peer-reviewed and accepted for publication. They are posted online prior to technical editing, formatting for publication and author proofing. The American Chemical Society provides “Just Accepted” as a free service to the research community to expedite the dissemination of scientific material as soon as possible after acceptance. “Just Accepted” manuscripts appear in full in PDF format accompanied by an HTML abstract. “Just Accepted” manuscripts have been fully peer reviewed, but should not be considered the official version of record. They are accessible to all readers and citable by the Digital Object Identifier (DOI®). “Just Accepted” is an optional service offered to authors. Therefore, the “Just Accepted” Web site may not include all articles that will be published in the journal. After a manuscript is technically edited and formatted, it will be removed from the “Just Accepted” Web site and published as an ASAP article. Note that technical editing may introduce minor changes to the manuscript text and/or graphics which could affect content, and all legal disclaimers and ethical guidelines that apply to the journal pertain. ACS cannot be held responsible for errors or consequences arising from the use of information contained in these “Just Accepted” manuscripts.



Two-Order Targeted Brain Tumor Imaging By Using an Optical/Paramagnetic Nanoprobe across the Blood Brain Barrier

Huihui Yan,[‡] Lu Wang,[†] Jiyao Wang,[‡] Xiaofu Weng,[§] Hao Lei,^{⊥,*} Xuxia Wang,[⊥] Lu Jiang,[¶] Jianhua Zhu,[†] Weiyue Lu[†], Xunbin Wei,^{§,*} and Cong Li^{†,*}

[†]Key Laboratory of Smart Drug Delivery, Ministry of Education & PLA, School of Pharmacy, Fudan University, Shanghai 201203, China, [‡]Department of Gastroenterology, Zhongshan Hospital affiliated to Fudan University, 180 Fenglin Rd., Shanghai 200032, China, [§]Med-X Research Institute and School of Biomedical Engineering, Shanghai Jiao Tong University, Shanghai 200030, China, [⊥]State Key Laboratory of Magnetic Resonance and Atomic and Molecular Physics, Wuhan Institute of Physics & Mathematics, The Chinese Academy of Sciences, Wuhan 430071, China, [¶]JHU ICMIC Program, The Russell H. Morgan Department of Radiology and Radiological Science, Johns Hopkins University School of Medicine, Baltimore, Maryland 21205, United States

*Address correspondence to: congli@fudan.edu.cn; xwei01@sjtu.edu.cn; leihao@wipm.ac.cn

Abstract: Surgical resection is a mainstay of brain tumor treatments. However, the completed excision of malignant brain tumor is challenged by its infiltration nature. Contrast enhanced magnetic resonance imaging (MRI) is widely used for defining brain tumor in clinic. However its ability for tumor visualization is hindered by the transient circulation lifetime, non-targeting specificity and poor blood brain barrier (BBB) permeability of the commercially available MR contrast agents. In this work, we developed a two-order targeted nanoprobe in which MR/optical imaging reporters, tumor vasculature targeted cyclic [RGDyK] peptides and BBB permeable Angiopep-2 peptides are labeled on PAMAM-G5 dendrimer. This nanoprobe is supposed to firstly target the $\alpha_v\beta_3$ integrin on tumor vasculatures. Increased local concentration of nanoprobe facilitates the association between BBB permeable peptides and the low-density lipoprotein receptor-related protein (LRP) receptors on the vascular endothelial cells, which further accelerates BBB transverse of the nanoprobe *via* LRP receptor mediated endocytosis. The nanoprobes that have penetrated BBB secondly

1
2
3
4 target the brain tumor because both $\alpha_v\beta_3$ integrin and LRP receptor are highly expressed on
5
6 the tumor cells. *In vivo* imaging studies demonstrated that this nanoprobe not only
7
8 efficiently crossed intact BBB in normal mice, but also precisely delineated the boundary of
9
10 orthotopic U87MG human glioblastoma xenograft with high target to background signal ratio.
11
12 Overall, this two-order targeted nanoprobe holds the promise to non-invasively visualize
13
14 brain tumors with uncompromised BBB and provides the possibility for the real-time optical
15
16 image-guided brain tumor resection during surgery.
17
18
19
20
21
22
23

24 **Keywords:** Brain tumor, Nanoprobe, Multimodal imaging, Blood Brain Barrier, Two-order
25
26 targeting
27
28
29
30

31 **Abbreviations:** GBM, glioblastoma multiforme; AA, anaplastic astrocytoma; MRI, magnetic
32
33 resonance imaging; CA, contrast agent; Gd, gadolinium; NIR, near-infrared; EPR, enhanced
34
35 permeability and retention; BCEC, brain capillary endothelial cell; Tf, transferrin; BBB, blood
36
37 brain barrier; LRP, low-density lipoprotein receptor-related protein; PDI, polydispersity index;
38
39 BTV, brain tumor vasculature, RAP, low-density lipoprotein receptor-associated protein; PI,
40
41 post-injection; T/N ratio, tumor to normal tissue ratio; MTT,
42
43 (3-(4,5-Dimethylthiazol-2-yl)-2,5-diphenyltetrazolium bromide; IC₅₀: the half maximal
44
45 inhibitory concentration.
46
47
48
49
50
51
52
53
54
55
56
57
58
59
60

1
2
3
4 Even the advances in tumor diagnosis and therapy have improved the survival of cancer
5
6 patients, malignant brain tumors continue to be the cause of a disproportionate morbidity and
7
8 mortality.¹ For example, the median survival of patients suffering aggressive glioblastoma
9
10 multiforme (GBM) is about 15 months and the anaplastic astrocytoma (AA) is 2–3 years.¹⁻²
11
12 The standard therapy for brain tumors involves surgical resection followed radiotherapy
13
14 or/and chemotherapy.³ However, malignant brain tumors are hard to eliminate completely
15
16 due to their heterogeneous and infiltrative nature, which leads to the precise resection of
17
18 tumor from the surrounding healthy brain tissue difficult during the surgery.⁴ Magnetic
19
20 resonance imaging (MRI) is a standard neuroimaging technique for pre-operative localization
21
22 of brain tumor.^{5,6} Gadolinium (Gd^{3+}) based MR contrast agents (CAs) such as Gd^{3+} -DTPA
23
24 (Magnevist[®]) are widely used to define tumor margin in clinic.⁷ These small molecular MR
25
26 CAs diffuse into the tumor bed where the blood brain barrier (BBB) is disrupted and lead to
27
28 MR signal enhancement. Unfortunately, the Gd approach is limited in that about 10% GBM
29
30 and 30% AA don't show any MR signal enhancement due to uncompromised BBB.⁸
31
32 Moreover, the transient circulation lifetime and non-targeting specificity of these CAs further
33
34 hinder their application. Therefore, the probes with BBB permeability, optimized circulation
35
36 lifetime and high targeting specificity are needed.
37
38
39
40
41
42
43
44
45
46
47
48

49 Nanoprobes demonstrate advantages in tumor imaging including the tunable circulation
50
51 lifetime,⁹ enhanced permeability and retention (EPR) effect that up-regulates intratumoral
52
53 delivery due to the high permeability of tumor vasculatures¹⁰⁻¹¹ and multivalent effect that
54
55 increases receptor targeting specificity by labeling multiple ligands on a single
56
57
58
59
60

1
2
3
4 nanoparticle.¹² Even previous works unambiguously showed the capability of nanoprobes
5
6 to visualize subcutaneous tumor xenografts *in vivo*,^{13,14} the performance of these
7
8 nanoprobes for brain tumor imaging is far from satisfaction because BBB prevents the
9
10 intracerebral delivery of almost all exogenous macromolecules.¹⁵ Receptor-mediated
11
12 transcytosis is a natural pathway through which the endogeneous proteins pass the BBB.¹⁶
13
14 Receptors presented on the brain capillary endothelial cells (BCECs) play active role in
15
16 mediating the intracerebral delivery of their corresponding ligands. Taking advantage of
17
18 this property, the receptor targeting ligands such as transferrin (Tf),¹⁷ rabies virus
19
20 glycoprotein peptide (RVG29)¹⁸ and snake neurotoxin candoxin peptide (CDX)¹⁹ were
21
22 functionalized into the nanoparticles to up-regulate their BBB permeability. Recently, Jia *et*
23
24 *al.* reported a drug delivery vector in which two different receptor-targeting ligands: Tf and
25
26 wheat germ agglutinin (WGA) were conjugated.²⁰ The improved therapeutic efficacy of this
27
28 nanoparticle to brain tumor was explained by the increased intratumoral delivery of the
29
30 chemotherapeutics resulted from the synergistic effect of Tf associated receptor-mediated
31
32 transcytosis and WGA associated adsorptive endocytosis. Above work demonstrated the
33
34 feasibility to enhance the brain tumor uptake of nanoparticles by increasing their BBB
35
36 traverse efficiency.
37
38
39
40
41
42
43
44
45
46
47
48

49 In this work, we developed a novel two-order targeted imaging strategy, which visualizes
50
51 brain tumor by up-regulating the BBB permeability and receptor targeting specificity of
52
53 nanoprobes (Fig. 1A). In this strategy, a nanoparticle labeled with MR/optical imaging
54
55 reporters, tumor vasculature targeting cyclic [RGDyK] peptides and BBB permeable
56
57
58
59
60

1
2
3
4 Angiopep-2 peptides was prepared. In the first step, this nanoprobe targets the tumor
5
6 neovasculatures that are abundant in tumor periphery. The increased local concentration of
7
8 nanoprobe facilitates the association between BBB permeable peptide and corresponding
9
10 receptor on the vascular endothelial cells, which accelerates BBB transverse of the
11
12 nanoprobe *via* the receptor mediated transcytosis. In the second step, the nanoprobe that
13
14 have penetrated BBB target the brain tumor directly because the corresponding receptors
15
16 are also highly expressed on tumor cells. This two-order targeting strategy realizes the
17
18 specific intratumoral delivery of imaging probes without disturbing normal function of the BBB.
19
20 $\alpha_v\beta_3$ integrin as a receptor for extracellular matrix proteins is over-expressed on the activated
21
22 endothelial cells of tumor neovasculatures, certain tumor cells, but not the normal
23
24 vasculatures.²¹ Therefore, $\alpha_v\beta_3$ integrin presents an ideal molecular target for tumor
25
26 diagnosis and therapy.²² Cyclic arginine-glycine-aspartic (RGD) tripeptide sequence shows
27
28 higher binding affinity to $\alpha_v\beta_3$ integrin (subnanomolar level)²³ and c[RGDyK] peptide was
29
30 chosen as the tumor vasculature targeting ligand here due to its convenience to be labeled
31
32 covalently on nanoparticles. Meanwhile, low-density lipoprotein receptor-related protein
33
34 (LRP) plays an active role in mediating the transport of numerous ligands across BBB
35
36 including lipoproteins, protease/protease inhibitor complexes and extracellular matrix
37
38 proteins.^{24,25} Angiopep-2, a 19 amino acid peptide derived from the common peptidic
39
40 sequence of the LRP protein ligands, demonstrates a much higher BBB transcytosis efficacy
41
42 than transferrin and its mother molecule aprotinin.^{26,27} Importantly, LRP receptors not only
43
44 express in BCECs, but also in many types of glioblastomas.²⁸ Therefore, angiopep-2 was
45
46 chosen as the BBB permeable ligand functionalized on the nanoprobe.
47
48
49
50
51
52
53
54
55
56
57
58
59
60

1
2
3
4
5 Like a “Great Wall” in brain, BBB protects the brain microenvironment from fluctuations in
6
7 concentrations of ions, metabolites, unwanted materials in the circulation system and keeps
8
9 the brain working under a perfect condition.²⁹ However, this defense proves to be a
10
11 nightmare during the treatment of brain tumor or other neurological diseases.^{30,31} Therefore,
12
13 the intracerebral delivery of the imaging/therapeutic agents by circumventing BBB is a
14
15 challenging but meaningful task. The objective of this work is to evaluate a novel imaging
16
17 strategy to non-invasively visualize the brain tumor with high sensitivity and target to
18
19 background signal ratio without the compromise to BBB.
20
21
22
23
24
25
26

27 **Result:**

28
29
30 **The Receptor Expression Level on Targeted Cells.** High expression of both $\alpha_v\beta_3$
31
32 integrin and LRP receptor in BCECs and brain cancer cells is a prerequisite for the success
33
34 of the two-order targeted imaging strategy. Receptor expression levels in the targeted cells
35
36 were immunoblotted by LRP1 and β_3 antibodies respectively. As shown in Fig. 1B, BCECs
37
38 demonstrated the immunoreactive bands at 85 and 110 kDa, the anticipated molecular
39
40 weights of LRP receptor and $\alpha_v\beta_3$ integrin. The receptor expression levels were also tested
41
42 in three human cancer cell lines including glioblastoma U87MG cells, prostate PC3 cells and
43
44 breast MDA-MB-231 cells. U87MG cells demonstrated the highest expression level of LRP
45
46 receptor. Densitometry studies showed that LRP receptor levels in U87MG and BCECs
47
48 were much higher than that in PC3 and MDA-MB-231 cells. Meanwhile, U87MG and BCEC
49
50 cells showed a comparable β_3 integrin expression level, but this receptor was not found in
51
52 PC3 and MDA-MB-231 cells.
53
54
55
56
57
58
59
60

1
2
3
4
5
6 **Design, Synthesis and Characterization of the Nanoprobcs.** The fifth generation (G5)
7
8
9 PAMAM dendrimer was chosen as a platform of the nanoprobcs due to its globular
10
11 architecture, identical molecular weight, optimized circulation lifetime and well-defined
12
13 reactive groups on the particle surface.^{32,33} Near-infrared (NIR) fluorophore Cy5.5 was
14
15 labeled on the dendrimer because tissue absorption and autofluorescence in this region
16
17 (650–900 nm) are low, which allows the NIR light to penetrate into deep tissue.³⁴ The
18
19 conjugated rhodamine was used to track the nanoprobcs in either cells or excised tissues
20
21 because Cy5.5 cannot be excited well under a conventional fluorescent microscope.
22
23 Gd³⁺-DOTA was chosen as the MR CAs functionalized on the nanoprobe due to its high
24
25 thermodynamic stability and kinetic inertness.³⁵ Both angiopep-2 and c[RGDyK] peptides
26
27 were labeled on the dendrimer through a PEG linker. This extended PEG linker not only
28
29 improves the biocompatibility of the nanoprobe, but also minimizes the steric hindrance of
30
31 the hyper-branched polymer to the targeting specificity of ligands.
32
33
34
35
36
37
38
39
40

41 The aiming nanoprobe **Den-RGD-Angio** labeled with both angiopep-2 and c[RGDyK]
42
43 peptides, control nanoprobcs **Den-RGD** modified with only c[RGDyK] peptides were
44
45 synthesized in Fig. 2A. Briefly, treatment of maleimide (Mal) and N-hydroxysuccinimidyl
46
47 (NHS) ester functionalized PEG derivative Mal-PEG^{2k}-NHS with c[RGDyK] offered
48
49 compound **1**, which further reacted with dendrimer to give **2**. The conjugation of NHS
50
51 esters of rhodamine, Cy5.5 and DOTA with **2** respectively gave **3** that then complexed with
52
53 Gd³⁺ ions to produce **Den-RGD**. The reaction between bis-functionalized PEG derivative
54
55
56
57
58
59
60

1
2
3
4 Mal-PEG^{2k}-NH₂ and N-succinimidyl 3-(2-pyridyldithio) propionate (SPDP) offered **4**. The
5
6 condensation between **4** and **2** resulted in **5**. The conjugation of NHS esters of rhodamine,
7
8 Cy5.5 and DOTA with **5** subsequently gave **6** that further reacted with peptide
9
10 TFFYGGSRGKRNNFKTEEYC followed a complexation with Gd³⁺ yielding **Den-RGD-Angio**.
11
12 The detail synthetic procedure of **Den-RGD** and **Den-RGD-Angio** was described in
13
14 supporting information. Meanwhile, synthesis of control nanoprobe **Den-Angio** labeled
15
16 with angiopep-2 peptides and **Den-PEG** without any targeting ligand was described in our
17
18 previous work.³⁶ The chemical structures of four nanoprobe were presented in Fig. 2B.
19
20
21
22
23
24
25

26
27 The physical parameters of those nanoprobe were listed in Table 1. The
28
29 hydrodynamic diameter of **Den-RGD-Angio** was determined as 15.6 nm, which was slightly
30
31 larger than that of control nanoprobe. The polydispersity index (PDI) of all nanoprobe
32
33 kept below 0.3 and every nanoprobe migrated as a single band in the fluorescence images
34
35 of the resolved sodium dodecyl sulfate-polyacrylamide gel electrophoresis (SDS-PAGE) (Fig.
36
37 S1). All nanoprobe showed the positive charges in the physiological pH, but the values
38
39 were much lower than that of unconjugated G5 dendrimer (Fig. S2). The molar ratio of
40
41 angiopep-2/c[RGDyK]/Gd³⁺-DOTA/dendrimer in **Den-RGD-Angio** was measured as
42
43 5/6/54/1. The molecular weights (MWs) of these nanoprobe were determined by
44
45 MALDI-TOF mass spectra (Fig. S3). All nanoprobe demonstrated similar longitudinal
46
47 relaxivity $r_{1\rho}$ values in a range of 7.1–7.4 mM⁻¹ s⁻¹/Gd³⁺.
48
49
50
51
52
53
54
55

56
57 **Cytotoxicity and Cellular Uptake Studies.** The cytotoxicities of the nanoprobe were
58
59
60

1
2
3
4 evaluated in U87MG cells *via* MTT assay. As shown in Fig. S4, all nanoprobe
5
6 demonstrated much lower cytotoxicities compared to the unmodified dendrimer. The IC_{50}
7
8 values of the nanoprobe were measured in a range of 6–30 μ M, which were at least 20
9
10 times higher than that of unmodified dendrimer (0.3 μ M). *In vitro* confocal fluorescence
11
12 microscopic imaging demonstrated the attachment of **Den-RGD-Angio** on the cell
13
14 membrane when the U87MG cells were treated with this nanoprobe for 15 min at 4 °C (Fig.
15
16 3A). Above experiment verifies the ligand/receptor association because the active cellular
17
18 uptake was minimized under low temperature. In order to evaluate the receptor targeting
19
20 specificity of **Den-RGD-Angio**, U87MG cells were treated with this nanoprobe in the
21
22 presence of the low-density lipoprotein receptor-associated protein (RAP) that was utilized
23
24 as a receptor competitor of LRP receptor and free c[RGDyK] peptide that was utilized as a
25
26 competitor of $\alpha_v\beta_3$ integrin. While the uptake of **Den-RGD-Angio** did not change upon the
27
28 treatment with c[RGDyK], no cellular uptake of this nanoprobe was monitored after the
29
30 pre-incubation of RAP (Fig. 3A). Above results indicated that LRP receptor played the
31
32 predominated role in the cellular uptake of **Den-RGD-Angio**. After 24 h incubation at 37 °C,
33
34 while **Den-RGD-Angio** distributed in whole cytoplasm as vesicular structures, **Den-PEG** was
35
36 sporadically located at the perinuclear areas (Fig. 3B). Internalizations of **Den-RGD** and
37
38 **Den-Angio** were evident, but their uptakes were obviously lower than that of
39
40 **Den-RGD-Angio**. Interestingly, quite different time-dependent internalization patterns of
41
42 the nanoprobe were observed by flow cytometry (Fig. 3C and Fig. S5). **Den-RGD-Angio**
43
44 and **Den-Angio** showed their fastest uptakes in the first 15 min. The initial uptake rates of
45
46 **Den-PEG** and **Den-RGD** were much lower than that of **Den-RGD-Angio**, however, a
47
48
49
50
51
52
53
54
55
56
57
58
59
60

1
2
3
4 sustained internalization of **Den-RGD** was observed. Average cellular fluorescence
5
6 intensity was quantified with an order of **Den-RGD-Angio** > **Den-Angio** > **Den-RGD** >
7
8 **Den-PEG** during the whole treatment procedure and the cellular uptake of **Den-RGD-Angio**
9
10 was found significantly higher than those of **Den-Angio** and **Den-PEG** ($P < 0.001$, $n = 4$) at
11
12 15 min, 1 h and 24 h post treatment (Fig. 3D).
13
14
15
16
17

18 ***In Vivo* Imaging Studies.** Dynamic T1-weighted MR images showed the prolonged
19
20 circulation lifetime of **Den-RGD-Angio** because the MR signal enhancement in intracerebral
21
22 vasculatures such as superior sagittal sinus and straight sinus lasted for more than 2 h
23
24 (upper panel of Fig. 4A). BBB permeability of **Den-RGD-Angio** was obvious with the
25
26 evidence of platelet-like hyperintense regions (positive contrast) in cortex at 24 h post
27
28 injection (PI). Average MR signal in the cortex increased 7.5% ($n = 4$) compared to its
29
30 pre-contrast values at 24 PI. BBB permeability of **Den-RGD-Angio** was further verified by
31
32 the *in vivo* NIR fluorescence imaging (Fig. 4C). The merged X-ray/optical image of
33
34 enlarged mouse head clearly indicated the location of this nanoprobe inside the skull that
35
36 was delineated by X-ray image. In contrast, the intracranial NIR fluorescence of **Den-PEG**
37
38 was remaining at the background level during the whole imaging process.
39
40
41
42
43
44
45
46
47
48

49 T1-weighted MR imaging demonstrated the feasibility of **Den-RGD-Angio** to visualize
50
51 the orthotopic U87MG glioblastoma xenograft *in vivo*. A heterogeneous MR signal
52
53 enhancement in tumor was observed as fast as 10 min PI. The tumor boundary was more
54
55 evident at 2 h PI and it correlated well with the H&E stained histological tissue section of the
56
57
58
59
60

1
2
3
4 identical brain tissues (low panel, Fig. 4A). Fig. 4B showed that the MR signal intensity ratio
5
6 between the tumor and surrounding normal neurological tissue (T/N ratio) kept increasing
7
8 after **Den-RGD-Angio** administration and reached its maximum value of 1.52 at 24 h PI.
9
10 **Den-RGD-Angio** also performed the highest NIR fluorescence associated T/N ratio in all
11
12 nanoprobe and its maximal value of 1.49 was measured at 24 h PI (Fig. 4C–D).
13
14
15
16
17
18

19 **Bio-distribution and Ex Vivo Imaging Studies.** *Ex vivo* NIR fluorescence images of the
20
21 excised normal mouse brain unambiguously demonstrated the accumulation of
22
23 **Den-RGD-Angio** in the cortex of normal brain (Fig. 5A). The average NIR fluorescence of
24
25 **Den-RGD-Angio** in the whole excised brain was measured as 17% (n = 3) higher than that
26
27 of **Den-PEG** (Fig. S6A). Microscopic fluorescent images of normal mouse brain sections
28
29 showed that **Den-RGD-Angio** and **Den-Angio** penetrated the brain capillaries and located in
30
31 the cortex parenchyma at 24 h PI (Fig. S6B). Whereas, no detectable intracerebral
32
33 deliveries of **Den-RGD** and **Den-PEG** were found. **Den-RGD-Angio** also showed the
34
35 highest T/N ratio in the excised brain bearing U87MG tumor xenograft (Fig. 5B) and the data
36
37 was measured as 5.6 at 24 h PI, which was much higher than the control nanoprobe (n = 3,
38
39 Fig. S6C). The bio-distribution data expressed as a percentage of injected dose/gram of
40
41 tissue (%ID/g) were evaluated in U87MG tumor bearing mice at 24 h PI of nanoprobe
42
43 labeled with radioactive ¹²⁵Iodide (Fig. 5C). All nanoprobe mainly located in the liver,
44
45 spleen and kidney. The intratumoral uptake of **Den-RGD-Angio** ($0.36 \pm 0.05\%$ ID g⁻¹) was
46
47 about 1.4, 1.7 and 2.6 times higher than that of **Den-RGD**, **Den-Angio** and **Den-PEG**
48
49 respectively. Fig. 5D demonstrated the white light and corresponding radioautographic
50
51
52
53
54
55
56
57
58
59
60

1
2
3
4 images of the tumor bearing brain sections at 24 h PI of the ^{125}I labeled nanoprobe. The
5
6 intratumoral delivery of nanoprobe was evident with the high radioactivity (displayed as
7
8 deep color) shown in the tumor area. **Den-RGD-Angio** gave the highest T/N ratio that was
9
10 measured as 1.41 at 24 h PI.
11
12

13
14
15
16 **Microscopic Immunofluorescence Imaging Studies.** Fig. 6A demonstrated the
17
18 fluorescence microscopic images of tumor bearing brain sections at 24 h PI of nanoprobe.
19
20 In contrast to the concentrated distribution of **Den-RGD-Angio** in entire tumor, **Den-PEG**
21
22 was only scatteredly located at the tumor boundary that can be defined by the fluorescence
23
24 images of nucleus stained by DAPI. The enlarged images indicated that **Den-RGD-Angio**
25
26 was internalized into the cancer cells and distributed as the vascular structures at the
27
28 perinucleus areas. The intratumoral deliveries of **Den-RGD** and **Den-Angio** were lower
29
30 than that of **Den-RGD-Angio** but significantly higher than that of **Den-PEG**. Fig. 6B
31
32 indicated the average cellular fluorescence intensities in the tumor and normal cells at 24 h
33
34 PI of nanoprobe. Compared to **Den-PEG**, the average fluorescence intensities in normal
35
36 neurological cells increased 1.2, 1.6 and 1.7 (15 slices analyzed from three tumors) times for
37
38 **Den-RGD**, **Den-Angio** and **Den-RGD-Angio** respectively. Remarkably, the average
39
40 fluorescence intensities of **Den-RGD**, **Den-Angio** and **Den-RGD-Angio** in brain tumor cells
41
42 were measured as 2.8, 2.7 and 4.5 times higher than that of **Den-PEG**.
43
44
45
46
47
48
49
50
51
52

53
54 This two-order targeted imaging of **Den-RGD-Angio** was further investigated by the
55
56 microscopic immunofluorescence imaging. Firstly, the targeting specificity of
57
58
59
60

1
2
3
4 **Den-RGD-Angio** to $\alpha_v\beta_3$ integrin was assessed at 2 and 24 h PI of the nanoprobe. The β_3
5
6 integrin was predominately located at the tumor margin with high vasculature density (Fig.
7
8 6C). The rhodamine fluorescence of **Den-RGD-Angio** colocalized well with the β_3 integrin
9
10 immunofluorescence at 2 h PI. However, the colocalization coefficient between the β_3
11
12 integrin and nanoprobe decreased from 0.74 at 2 h PI to 0.26 (18 slices analyzed from three
13
14 tumors) at 24 h PI due to the continued uptake of this nanoprobe in the tumor core area (Fig.
15
16 6D). The targeting specificity of nanoprobe to the LRP receptors was also studied. The
17
18 LRP receptors are heterogeneously located in the brain tumor and the colocalization
19
20 coefficient between LRP receptor and **Den-RGD-Angio** was determined as high as 0.86 at 2
21
22 h PI (Fig. 6D). Interestingly, the immunofluorescence of LRP receptor in the tumor core
23
24 area disappeared and the colocalization coefficient reduced to 0.07 (18 slices analyzed from
25
26 three tumors) at 24 PI.
27
28
29
30
31
32
33
34
35

36 **Discussion:**

37
38
39 Poor BBB permeability of the imaging/therapeutic agents is a bottleneck that limits the
40
41 successful brain tumor diagnosis and treatment. In proof-of-principle, we put forward a
42
43 novel two-order targeted nanoprobe to non-invasively image the brain tumor by
44
45 circumventing BBB *in vivo*. The up-regulated BBB traversing efficacy of this nanoprobe
46
47 results from: (1) multivalent effect that boosts the avidity to the targeted receptor on brain
48
49 tumor vasculatures. For example, Josephson *et al.* reported the binding affinity of the
50
51 nanoparticle modified with twenty c[RGDfK] peptides was 71 times higher compared to that
52
53 of the free peptide;³⁷ (2) high local ligand concentration effect that up-regulates the receptor
54
55
56
57
58
59
60

1
2
3 mediated transcytosis. DeSimone *et al* reported that the cellular uptake of the PRINT
4 nanoparticle was proportional to the density of the labeled Tf.³⁸ Therefore, a combination of
5
6
7
8 the multivalent effect and the high local ligand concentration effect can remarkably increase
9
10
11 the BBB permeability of nanoprobes.
12
13
14
15

16 Higher permeability of tumor vasculature provided a natural selection process to allow
17
18 the nanoparticles to extravasate into the tumor interstitium but not the normal tissues.³⁹
19
20 However, brain tumor vasculature (BTV) retains some features of the BBB such as tight
21
22 interendothelial junctions and transendothelial channels.¹⁵ For example, Sarin *et al.* found
23
24 the upper limit of the pore size in BTV would be less than 20 nm in diameter,³³ which is much
25
26 smaller than that of extracranial tumors up to 1–5 μm .³⁹ Furthermore, the nanoprobes
27
28 smaller than 5 nm are also not suitable for brain tumor imaging because their fast excretion
29
30
31
32
33
34
35
36
37
38
39
40
41
42
43
44
45
46
47
48
49
50
51
52
53
54
55
56
57
58
59
60
via renal filtration results in their transient residence in blood pool.⁴⁰ In this work, the
diameters of the nanoprobes are in a range of 11–16 nm that are small enough to traverse
BTV but bigger enough to achieve the prolonged circulation lifetime. The reduced
cytotoxicity of the nanoprobes compared to the unmodified dendrimer can be explained by
their lower positive charges that reduce the non-specific accumulation of nanoprobe in the
normal tissues.⁴¹ However, the residue positive charge of nanoprobes would potentially
facilitate their intratumoral uptake *via* the electrostatic interaction between the cationic
nanoprobe and the negative charged sulfated proteoglycans over-expressed on the cancer
cells.⁴² High sensitivity of NIR fluorescence imaging can compensate the inherent shortage
of MRI by using the multimodal nanoprobes, and it is promising to generate the images with

1
2
3
4 high spatially resolution as well as the sensitivity. Meanwhile, due to the numerous MR
5
6 chelators labeled on the nanoprobe, the overall relaxivity of the nanoprobe can be as high as
7
8
9 $355 \text{ mM}^{-1} \text{ s}^{-1}$ /nanoprobe, which benefits to generate detectable MR signal even nanoprobe
10
11 concentration is low in brain tissues.
12

13
14
15
16 *In vitro* competition studies clearly indicated the dominated role of LRP receptor played in
17
18 the cellular uptake of **Den-RGD-Angio**. Actually, the maximum cellular uptake velocity of
19
20 **Den-RGD-Angio** performed in the beginning of treatment can be explained by the
21
22 overwhelming ligand/receptor association that is much faster than the active internalization.
23
24 The highest cellular uptake rate of **Den-RGD-Angio** in the whole incubation period
25
26 presumably results from synergistic receptor targeting effect of angiopep-2 and c[RGDyK]
27
28 peptides.
29
30
31
32

33
34
35
36 BBB permeability of **Den-RGD-Angio** was unambiguously verified by *in vivo* MR/optical
37
38 imaging, *ex vivo* optical imaging as well as microscopic imaging studies. The role of LRP
39
40 receptor mediated transcytosis played in the intracerebral delivery is obvious because
41
42 MR/NIR fluorescence signal enhancements in cortex were only observed after the injection
43
44 of nanoprobe modified with angiopep-2 ligand. Interestingly, even angiopep-2 densities
45
46 on **Den-RGD-Angio** and **Den-Angio** were the same, **Den-RGD-Angio** showed a higher
47
48 BBB traverse efficiency compared to **Den-Angio**. Milner et al reported the presence of
49
50 $\alpha_v\beta_3$ integrin in the BCECs.⁴³ The synergistic targeting effect of **Den-RGD-Angio** found in
51
52 cell culture studies may also increase its local concentration in BCECs, which further
53
54
55
56
57
58
59
60

1
2
3 accelerates its BBB traverse efficiency. Due to the high tissue penetration capability of NIR
4
5
6 fluorescence, the intracerebral delivery of nanoprobe was detected by NIR optical imaging
7
8
9 as early as 2 h PI, which provided a convenient and sensitive way to dynamically track the
10
11 intracerebral delivery of nanoprobe.
12
13

14
15
16 Both MR and optical imaging demonstrated the intratumoral delivery of all four nanoprobe
17
18 *in vivo*. Due to the EPR effect, all nanoprobe can enter the tumor by extravasating the
19
20 impaired BBB. However, compared to the controls, **Den-RGD-Angio** not only offered the
21
22 highest T/N ratio, but also precisely delineated the tumor boundary. The perfect tumor
23
24 boundary correlation between the *in vivo* MR image and the *ex vivo* histological images
25
26 indicates the feasibility of this nanoprobe to pre-surgically locate the brain tumor.
27
28
29 Recently, Zhang et al. reported an iron oxide nanoparticle based T2-weight MR probe
30
31 modified with chlorotoxin (CTX) as the targeting ligand.⁴⁴ Even this nanoprobe successfully
32
33 visualized the transgenic ND2:SmoA1 brain tumor *in vivo*, the neoplastic tissue cannot be
34
35 precisely defined until 48 h PI due to the slow extravasation rate of the nanoprobe.
36
37
38 Furthermore, the “negative contrast” signal induced by the iron oxide particles may mislead
39
40 the clinical diagnosis because endogenous tissues such as necrosis, calcification,
41
42 hemorrhage or metal deposition are also presented as “hypointense areas” in MRI.⁴⁵
43
44
45 Therefore, our nanoprobe with fast intratumoral delivery rate and “positive” signal
46
47 enhancement in neoplastic tissues is more desirable to the radiologist. Furthermore, due to
48
49 the extremely high T/N ratio of **Den-RGD-Angio** performed in the *ex vivo* optical imaging
50
51 studies, this nanoprobe holds promise in the real-time optical imaging guided surgery to
52
53
54
55
56
57
58
59
60

1
2
3 completely remove the neoplastic tissues with the minimized impairments to the surrounding
4
5 normal neurological tissues.
6
7

8
9
10 As indicated in the microscopic immunofluorescence studies, high colocalization
11
12 coefficients between **Den-RGD-Angio** and the LRP receptor as well as β_3 integrin at 2 h PI
13
14 indicated the involvement of both receptors in the targeted delivery of nanoprobe.
15
16 Additionally, in contrast to the location of **Den-PEG** at the tumor periphery, **Den-RGD-Angio**
17
18 was distributed in the whole tumor area and internalized into cytoplasm. Above
19
20 experimental results support the assumed two-order targeted imaging strategy. At 24 h PI,
21
22 remarkably reduced co localization coefficients may be interpreted by the “receptor
23
24 occupation effect”,⁴⁶ in which the receptors on cancer cells were preoccupied by the
25
26 nanoprobe and hardly to be immunostained by corresponding antibodies. Compared to
27
28 the **Den-PEG**, the average cellular fluorescence intensities of **Den-RGD-Angio** and
29
30 **Den-Angio** in normal brain tissues increased to 67–75%, which is a solid evidence of the
31
32 LRP-mediated transcytosis *in vivo*. Overall, the combination of EPR effect, up-regulated
33
34 BBB permeability, and the two-order targeting strategy jointly contributes to the high T/N
35
36 ratio of **Den-RGD-Angio**.
37
38
39
40
41
42
43
44
45
46
47

48 **Conclusion**

49
50 Overall, this work developed a novel two-order targeted imaging strategy that successfully
51
52 visualized orthotropic brain tumor xenograft with high sensitivity and target to background
53
54 signal ratio *in vivo*. This multimodal nanoprobe not only demonstrated the feasibility to
55
56 pre-operatively localize brain tumors by both MRI and optical imaging, but also provided a
57
58
59
60

1
2
3 potential solution to delineate the malignant tumor with uncompromised BBB. Additionally,
4
5 due to its extraordinarily high T/N ratio performed under the *ex vivo* condition, this nanoprobe
6
7
8 holds a promise in NIR optical image-guided brain tumor resection during the surgery.
9

10 11 12 13 **MATERIALS AND METHODS**

14
15
16 **Materials.** All chemicals were analytical grade from Aladdin Reagent (Shanghai, China)
17
18 unless otherwise specified. PAMAM G5 dendrimer (77.35 mg/mL in MeOH) was purchased
19
20 from DendritechInc (Midland, USA). Rhodamine-NHS, Cy5.5-NHS and SPDP were from
21
22 Thermofisher Scientific (NY , USA). Fetal bovine serum (FBS), penicillin, streptomycin,
23
24 Alexa Fluo 488 or horseradish peroxidase (HRP) labeled goat anti-rabbit secondary
25
26 antibodies were from Invitrogen (Carlsbad, USA). Rabbit anti-mouse/human β -actin, β_3
27
28 integrin and LRP-1 primary antibodies were from Epitomics (Burlingame, USA).
29
30 Maleimide-PEG^{2k}-NHS and PEG^{2K}-NHS were from JenKem Technology (Beijing, China).
31
32 DOTA-NHS was prepared according to previous report.⁴⁷ Gd₂(CO₃)₃, DAPI, Bolton-Hunter
33
34 reagent and MTT were purchased from Sigma-Aldrich (St. Louis, USA). Isoflurane was
35
36 from Baxter Healthcare Corporation (New Providence, USA).
37
38
39
40
41
42
43
44
45

46
47 **Western Blot Studies.** Approximately 3×10^6 cells at 80% confluence were
48
49 homogenized with lysis buffer containing protease inhibitors. 80 μ g total protein determined
50
51 by a modified Lowry assay (Bio-Rad) were resolved on a 7% SDS-PAGE. The gels were
52
53 transferred to polyvinylidenedifluoride membranes, blocked, cut and incubated with β -actin
54
55 (1:50000) or β_3 integrin (1:1000) or LRP-1 (1:20000) primary antibodies. The membrane
56
57
58
59
60

1
2
3 was incubated with HRP labeled goat anti-rabbit secondary antibody (1:2000) and visualized
4
5
6 by using the Supersignal WestPico chemiluminescent substrate kit (Pierce Biotechnology,
7
8
9 USA).

10
11
12
13 **Cell Culture Studies.** U87MG, PC3, MDA-MB-231 and BCECs (ATCC) were cultured as
14
15 recommended by the supplier.
16
17

18
19
20
21 **Confocal Fluorescence Microscopic Imaging.** Fluorescence microscopic images were
22
23 collected on a Zeiss LSM 510 META confocal laser scanning microscope (Carl Zeiss,
24
25 Germany) by using a 40× oil immersion lens. DAPI was excited with a 405 nm laser and the
26
27 emission was detected with a photomultiplier by a 420–480 nm band-pass filter. Alexa Flour
28
29 488 was excited with a 495 nm laser and emission was detected by a second photomultiplier
30
31 using a 505–550 nm band-pass filter. Rhodamine was excited with a 543 nm laser and the
32
33 emission was detected by a third photomultiplier using a 560 nm band-pass filter.
34
35
36
37
38
39

40
41 **Flow cytometry.** U87MG cells with 80% confluence were treated with 1.0 μM nanoprobe
42
43 in which the rhodamine was replaced by fluorescein. At the end of incubation, the cells
44
45 were washed, centrifuged, fixed and analyzed by BD FACSAria (BD Biosciences, USA)
46
47 equipped with a 488 nm Ar-Ion laser.
48
49
50
51

52
53
54 **Tumor Implantation.** All animal experiments were carried out in accordance with
55
56 guidelines approved by the ethics committee of Fudan University, Shanghai, China.
57
58
59
60

1
2
3
4 U87MG cells (5.0×10^5) were inoculated into the right striatum (1.8 mm lateral, 0.6 mm
5
6 anterior to the bregma and 3.0 mm of depth) of male Balb/c nude mice by using a
7
8 stereotactic fixation device with mouse adaptor. The intracranial tumors with a diameter of
9
10 0.5–1.0 mm were ready for imaging after inoculation for 14–18 days.
11
12

13
14
15
16 ***In vivo* MRI Studies.** *In vivo* MR imaging was carried out on a Biospec 47/30 MRI scanner
17
18 (Bruker Inc., MA). The mice were anesthetized with isoflurane and their heads were placed
19
20 into a home-built solenoid coil. Mouse respiration was continuously monitored by a Bruke
21
22 PhysioGard system. Dynamic T1-weighted images of the brain were collected before and
23
24 after bolus administration of nanoprobe with a dose of 0.05 mmol/kg [Gd^{3+}] in a 0.25 mL PBS
25
26 *via i.v.*. Coronal images of the brain sections with 1.0 mm thickness were acquired with a
27
28 spin-echo pulse sequence [field of view (FOV): 2 cm \times 2 cm, matrix size: 128 \times 128, TR =
29
30 300 ms, TE = 11 ms, and number of average (NOV) = 8]. The intensity enhancement (IE)
31
32 of region of interest (ROI) at time point t is expressed by $\text{IE} = (\text{RI}(t) - \text{RI}(0))/\text{RI}(0) \times 100\%$,
33
34 where RI(t) and RI(0) correspond to the normalized signal intensities measured at time point
35
36 t and pre-injection.
37
38
39
40
41
42
43
44
45

46
47 ***In vivo* and *ex vivo* Optical Imaging Studies.** Optical images were acquired on a Kodark
48
49 Multispectral Imaging System equipped with a 750 nm excitation filter and a 800 nm
50
51 emission band pass filter set. All X-ray images were acquired by using 0.2 s exposure time
52
53 and NIR fluorescence images were acquired using 0.5 s exposure time (FOV = 6.4 or 12.8
54
55 cm; f/stop, 4; bin, high resolution). The fluorescence intensities were quantified by ImageJ
56
57
58
59
60

1
2
3
4 software (NIH).
5
6
7

8
9 **Bio-distribution.** Nanoprobes were radiolabeled with ^{125}I isotope by using the
10 Bolton-Hunter reagent (Pierce Biotech., USA). U87MG tumor bearing mice were randomly
11 divided into four groups and injected with [^{125}I] labeled nanoprobes (3.0×10^5 Bq/mouse) *via*
12 *i.v.* The mice were sacrificed at 24 h PI and perfused with saline. Selected organs were
13 excised, weighed and the radioactivity was counted with an automatic γ -counter. The
14 biodistribution data were presented as percentage of the injected dose per gram (%ID/g).
15
16
17
18
19
20
21
22
23
24
25

26 **Autoradiography Studies.** After bio-distribution studies, mouse brains were excised,
27 cryo-sectioned with a thickness of 20 μm . The autoradiogram images were collected by a
28 cyclone pulse storage phosphor system (Perkin Elmer, USA) with an exposure time of 24 h.
29 The white light pictures of these brain sections were taken by a Leica MZ75 (Leica Inc.,
30 Germany) high-performance stereomicroscope equipped with 2.5 X plano objective.
31
32
33
34
35
36
37
38
39
40

41 **Histological and Immunohistological Staining.** Tumor bearing brains were fixed,
42 dehydrated, and sectioned at least 15 sections per brain with a thickness of 20 μm . The
43 sections from each brain were divided for three groups. Group one were stained with
44 hematoxylin and eosin (H&E); group two were stained with β_3 integrin primary antibody
45 followed the fluorophore labeled secondary antibody and DAPI at last; group three were
46 stained by LRP-1 primary antibody followed the secondary antibody and DAPI at last.
47
48
49
50
51
52
53
54
55
56

57 **Statistical Analysis.** Values presents mean \pm SD when the sample number is above 3
58
59
60

1
2
3
4 (n > 3). Statistical differences were evaluated with two tailed corrected Student's *t* test
5
6 (SPSS, IBM); *P* < 0.05 was considered significant. Values are presented as mean and data
7
8 range (from minimum value to maximum value) when the sample number is 3 (n = 3).
9
10

11 12 13 14 **Acknowledgements.**

15
16
17 This work was supported by the National Basic Research Program of China (973 program,
18
19 2011CB910404), the National Natural Science Foundation of China (No. 30900353,
20
21 81171384, 20975027), and Program for New Century Excellent Talents in University Award
22
23 (NCET-08-0131). We thank the helpful discussion with Prof. X. Y. Feng and Prof. C. Jiang.
24
25
26
27
28

29 **Supporting Information Available:**

30
31
32 Details of nanoprobe synthesis, characterization, *in vitro* cytotoxicity studies, Figs.
33
34 S1–S6, NMR and MS spectra. This material is available free of charge *via* the Internet at
35
36 <http://pubs.acs.org>.
37
38
39
40
41
42
43
44
45
46
47
48
49
50
51
52
53
54
55
56
57
58
59
60

Table and Figures

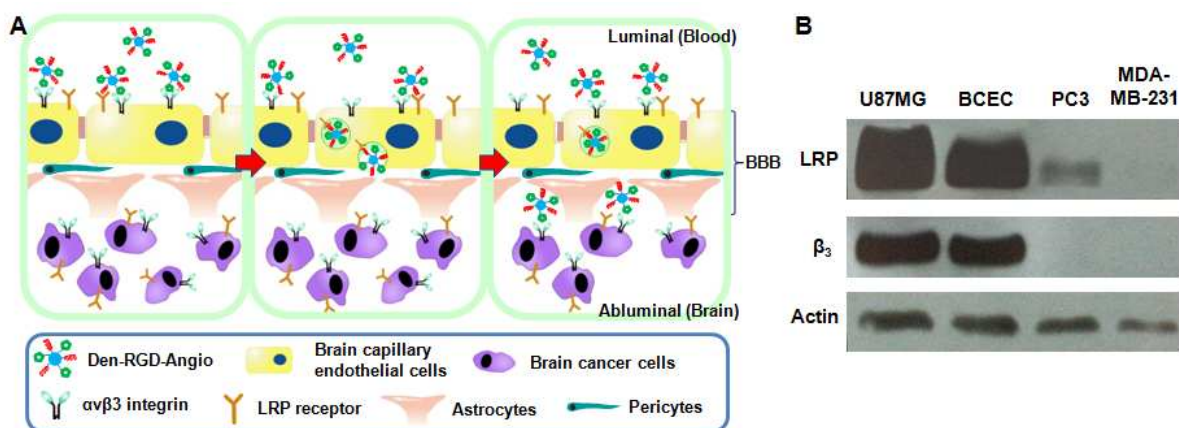


Figure 1. Design of the two-order targeted nanoprobe for brain tumor imaging. (A) Overview of two-order targeted brain tumor imaging strategy. The nanoprobe firstly targets the $\alpha_v\beta_3$ integrin on tumor vasculatures. After binding with nearby LRP receptors, the nanoprobe traverses BBB *via* LRP receptor-mediated transcytosis and finally targets tumor cells directly. (B) Western blot shows the over-expression of both $\alpha_v\beta_3$ integrin and LRP receptor in human glioblastoma U87MG cancer cells and BCECs.

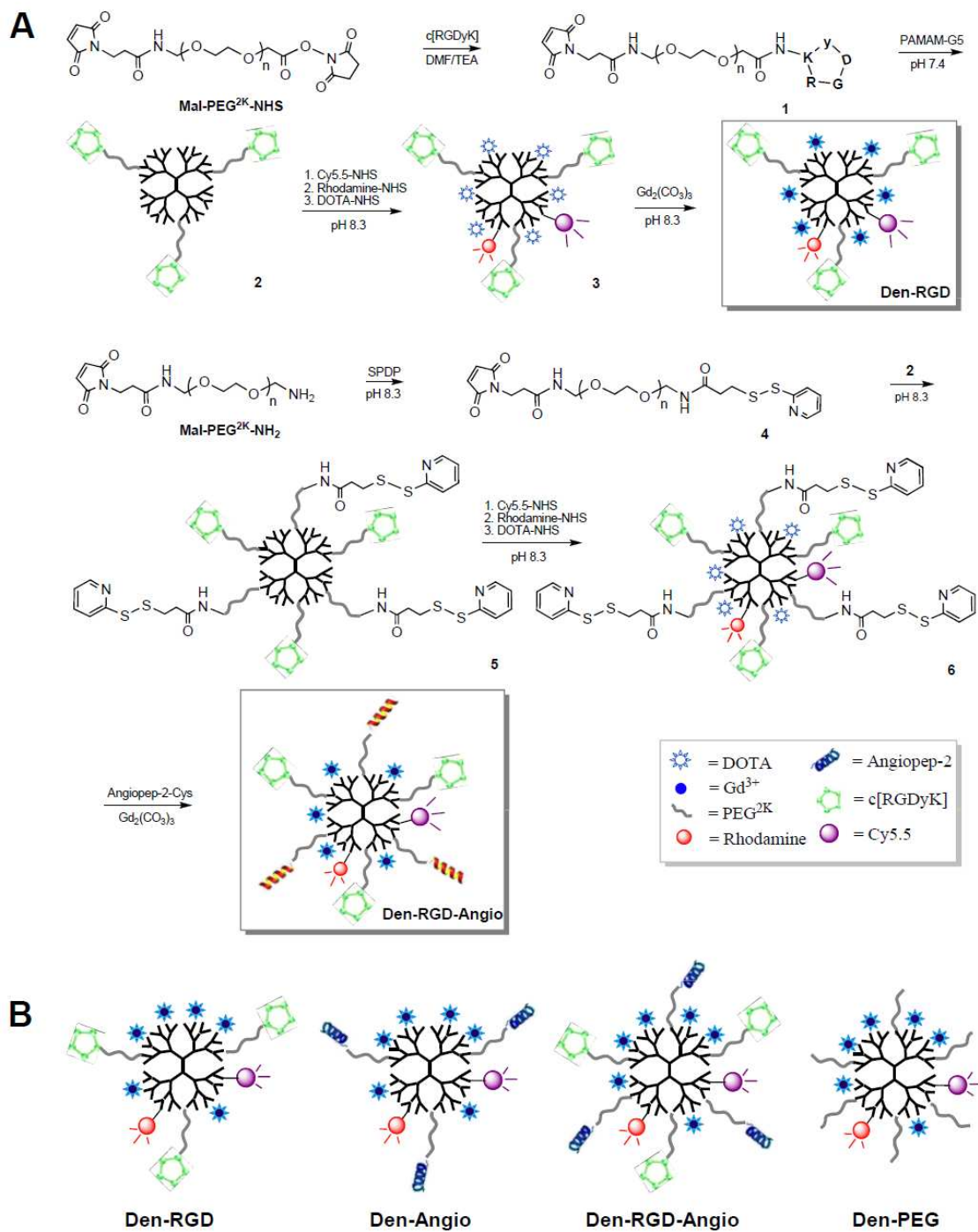


Figure 2. (A) Synthetic steps of nanoprobes **Den-RGD** and **Den-RGD-Angio**. (B) Schematics of the aiming and control nanoprobes.

Table 1. Physical parameters of the nanoprobe

Nanoprobe	d (nm) ^a	PDI ^a	ζ (mV) ^a	Gd% ^b	r_{1p} (mM ⁻¹ s ⁻¹) ^c	MW (kDa) ^d
Den-PEG	11.5	0.258	16.7	12.5	7.4 ± 0.4	82
Den-RGD	13.2	0.193	10.4	9.6	7.1 ± 0.3	81
Den-Angio	13.3	0.287	11.6	9.4	6.9 ± 0.4	83
Den-RGD-Angio	15.6	0.224	8.6	9.6	7.1 ± 0.2	91
G5 Dendrimer	7.1	0.157	21.5	n.d.	n.d.	30

^a Diameters (d), polydispersity index (PDI) and Zeta potentials (ζ) were measured by dynamic light scattering (DLS). ^b Gadolinium concentrations (Gd%) were measured by inductively coupled plasma atomic emission spectroscopy (ICP-AES). ^c T1-weighted relaxivities (r_{1p}) were determined on 4.7 T MRI at 25 °C. ^d Molecular weights (MW) were measured by MALDI-TOF MS.

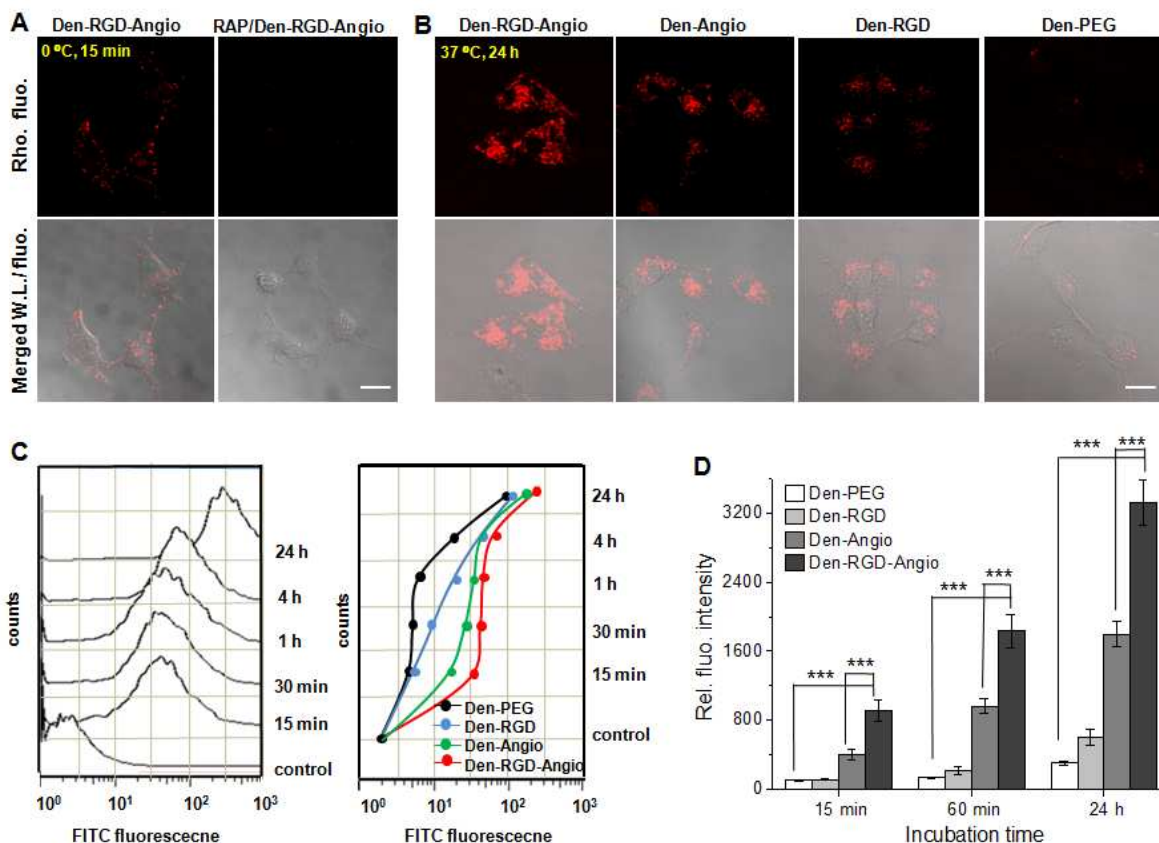


Figure 3. Den-RGD-Angio demonstrated a higher cellular uptake efficacy than the control nanoprobes in U87MG cells. (A) Confocal fluorescence microscopic images of the live cells treated with 1.0 μM **Den-RGD-Angio** for 15 min or pre-treated with 2.0 μM RAP for 30 min followed the nanoprobe treatment. Above experiments were conducted at 4 $^{\circ}\text{C}$. Rhodamine fluorescence was displayed in red. (B) Microscopic fluorescence images of the live cells treated with 1.0 μM selected nanoprobe for 24 h at 37 $^{\circ}\text{C}$. Scale bar, 15 μm . (C) Time-dependent flow cytometries of the cells treated with **Den-RGD-Angio** (1.0 μM , left panel) and time-dependent cellular fluorescence intensity curves after treatment of nanoprobe (1.0 μM , right panel). (D) Mean cellular fluorescence intensities after nanoprobe treatment for 15 min, 1 h and 24 h at 37 $^{\circ}\text{C}$. The values represent mean \pm SD ($n = 4$). (***) $P < 0.001$.

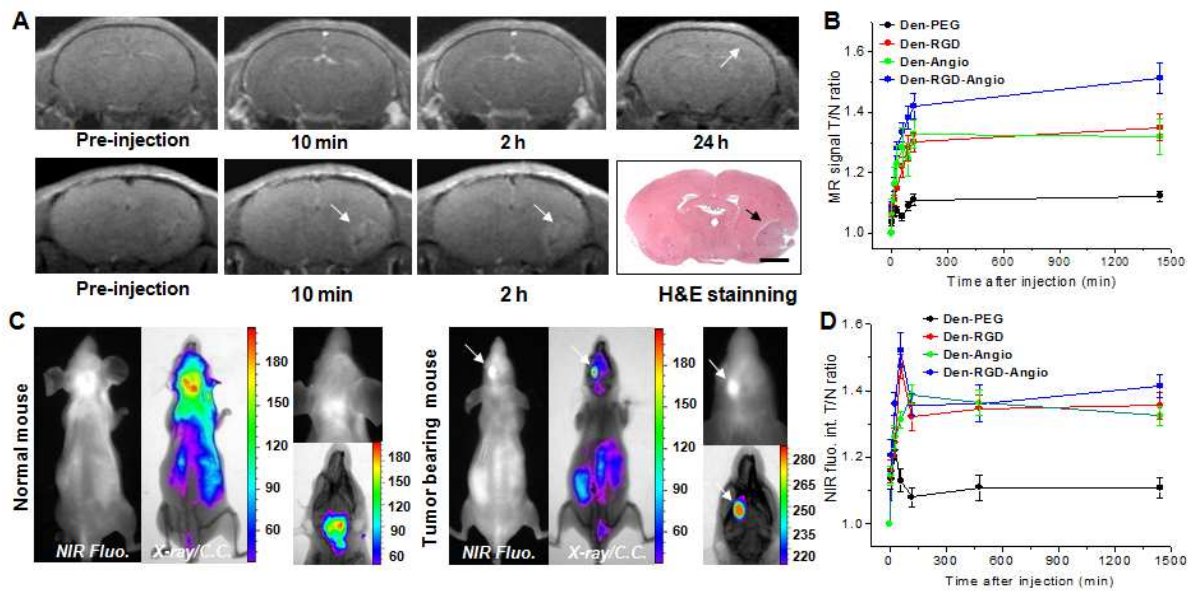


Figure 4. Den-RGD-Angio demonstrated high BBB permeability and T/N ratio *in vivo*. (A) Representative T1-weighted MR images of normal mouse brain (upper panel, arrow points to the cortex) and tumor bearing brain (lower panel, arrows point to the tumor) before and at selected time PI of **Den-RGD-Angio** (0.05 mmol/kg [Gd^{3+}], *i.v.*). Histological H&E staining verified the tumor boundary in MRI (Bar, 2.0 mm). (B) *In vivo* time-dependent MR signal associated T/N ratio before and PI of nanoprobe ($n = 4$). Points present mean values and bars present the maximum and minimum values (data range). (C) Representative NIR fluo. and X-ray/color coded NIR fluo. images of the normal mouse (left panel) and brain tumor bearing mouse (right panel) at 24 h PI of **Den-RGD-Angio** (5.0 nmol/mouse based on dendrimer). (D) *In vivo* time-dependent NIR fluorescence T/N ratio ($n = 3$). Points present mean values and bars present the data range.

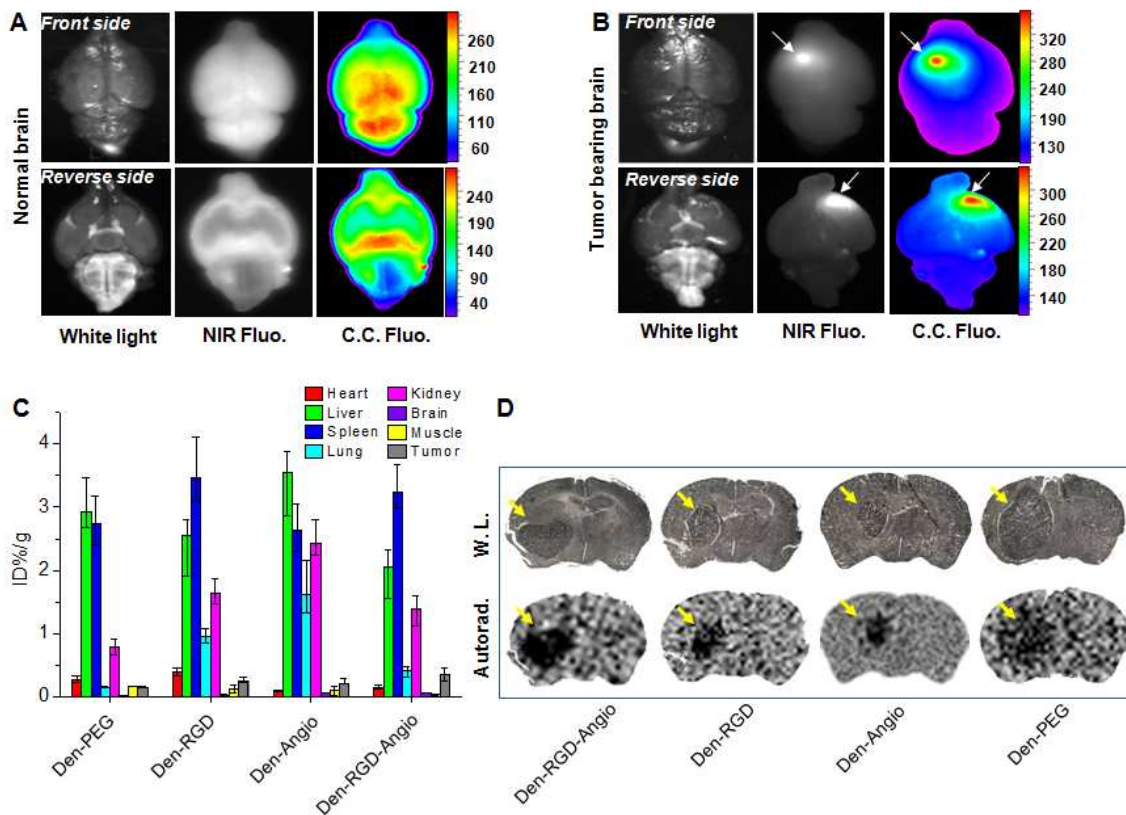


Figure 5. Bio-distribution and *ex vivo* imaging studies verified the high T/N ratio of **Den-RGD-Angio**. Representative white light, NIR fluorescence and color coded fluorescence images of normal mouse brain (A) and tumor bearing mouse brain (B) at 24 h PI of **Den-RGD-Angio**. Arrow points to the tumor. (C) Biodistribution of nanoprobe labeled with ^{125}I radioactive isotope (1.8×10^5 Bq/mouse) in tumor bearing mice ($n = 3$) at 24 h PI. Columns present mean values and bars present the data range. (D) Representative white light microscopic images and autoradiographic images of tumor bearing brain sections at 24 h PI of the radioactive nanoprobe. Arrows point to the tumors.

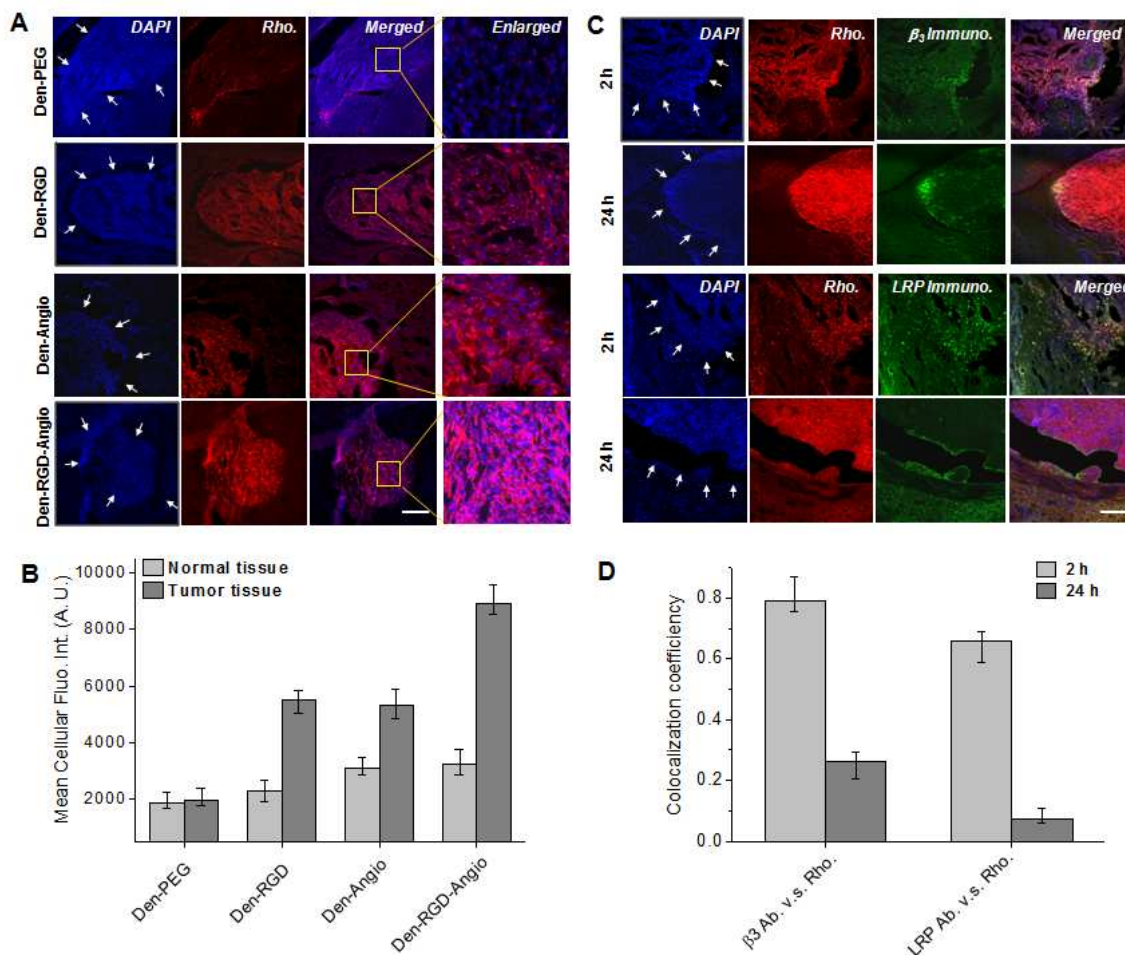


Figure 6. $\alpha_v\beta_3$ integrin and LRP receptor are involved in the two-order targeted imaging strategy. (A) Representative confocal microscopic fluorescence images of tumor bearing brain sections at 24 h PI of nanoprobe (5.0 nmol/mouse). Rhodamine in nanoprobe was displayed in red and the nuclei stained with DAPI were displayed in blue. Tumor boundary was indicated by the arrows. Scale bar, 200 μm . (B) Intracellular fluorescence intensity at 24 h PI of the nanoprobe. The data were quantified by normalizing the gross rhodamine fluorescence with the number of nuclear in the indicated areas. Columns present mean values and bars present the data range. (Randomly selected 15 images analyzed from 3 tumors after a nanoprobe injection). (C) Representative microscopic fluorescence images of tissue sections immunohistologically stained with β_3 integrin antibody (upper panel) and LRP antibody (lower panel) at 2 and 24 h PI of **Den-RGD-Angio**. The immunofluorescence was displayed in green. Scale bar, 200 μm . (D) Colocalization coefficients between the nanoprobe fluorescence and the immunofluorescence in the tumor at 2 and 24 h PI of **Den-RGD-Angio**. (Randomly selected 18 images analyzed from 3 tumors after a nanoprobe injection).

References:

1. Wen, P. Y.; Kesari, S., Malignant Gliomas in Adults. *N. Engl. J. Med.* **2008**, *359*, 492–507.
2. Huse, J. T.; Holland, E. C., Targeting Brain Cancer: Advances in the Molecular Pathology of Malignant Glioma and Medulloblastoma. *Nat. Rev. Cancer* **2010**, *10*, 319–331.
3. Laws, E. R.; Parney, I. F.; Huang, W.; Anderson, F.; Morris, A. M.; Asher, A.; Lillehei, K. O.; Bernstein, M.; Brem, H.; Sloan, A. *et al.* Survival Following Surgery and Prognostic Factors for Recently Diagnosed Malignant Glioma: Data from the Glioma Outcomes Project. *J. Neurosurg.* **2003**, *99*, 467–473.
4. Donahue, M. J.; Blakeley, J. O.; Zhou, J.; Pomper, M. G.; Lattera, J.; van Zijl, P. C., Evaluation of Human Brain Tumor Heterogeneity Using Multiple T1-Based MRI Signal Weighting Approaches. *Magn. Reson. Med.* **2008**, *59*, 336–344.
5. Zhou, J.; Tryggstad, E.; Wen, Z.; Lal, B.; Zhou, T.; Grossman, R.; Wang, S.; Yan, K.; Fu, D. X.; Ford, E. *et al.* Differentiation between Glioma and Radiation Necrosis Using Molecular Magnetic Resonance Imaging of Endogenous Proteins and Peptides. *Nat. Med.* **2011**, *17*, 130–134.
6. Weber, M. A.; Giesel, F. L.; Stieltjes, B., MRI for Identification of Progression in Brain Tumors: from Morphology to Function. *Expert Rev. Neurother.* **2008**, *8*, 1507–1525.
7. Giesel, F. L.; Mehndiratta, A.; Essig, M., High-Relaxivity Contrast-Enhanced Magnetic Resonance Neuroimaging: A Review. *Eur. Radiol.* **2010**, *20*, 2461–2474.
8. Scott, J. N.; Brasher, P. M.; Sevick, R. J.; Rewcastle, N. B.; Forsyth, P. A., How Often Are Nonenhancing Supratentorial Gliomas Malignant? A Population Study. *Neurology* **2002**, *59*, 947–949.
9. Whitesides, G. M., The 'Right' Size in Nanobiotechnology. *Nat. Biotechnol.* **2003**, *21*, 1161–1165.
10. Maeda, H., Tumor-Selective Delivery of Macromolecular Drugs *via* the EPR Effect: Background and Future Prospects. *Bioconjug. Chem.* **2010**, *21*, 797–802.
11. Torchilin, V., Tumor Delivery of Macromolecular Drugs Based on the EPR Effect. *Adv. Drug. Deliv. Rev.* **2011**, *63*, 131–135.
12. Hong, S.; Leroueil, P. R.; Majoros, I. J.; Orr, B. G.; Baker, J. R., Jr.; Banaszak Holl, M. M., The Binding Avidity of A Nanoparticle-Based Multivalent Targeted Drug Delivery Platform. *Chem. Biol.* **2007**, *14*, 107–115.
13. Janib, S. M.; Moses, A. S.; MacKay, J. A., Imaging and Drug Delivery Using Theranostic Nanoparticles. *Adv. Drug. Deliv. Rev.* **2010**, *62*, 1052–1063.
14. Li, C.; Xia, J.; Wei, X.; Yan, H.; Si, Z.; Ju, S., pH-Activatable Near-Infrared Fluorescence Nanoprobe Imaging Tumors by Sensing the Acidic Microenvironment. *Adv. Funct. Mater.* **2010**, *20*, 2222–2230.
15. Black, K. L.; Ningaraj, N. S., Modulation of Brain Tumor Capillaries for Enhanced Drug Delivery Selectively to Brain Tumor. *Cancer Control* **2004**, *11*, 165–173.
16. Shi, N.; Boado, R. J.; Pardridge, W. M., Receptor-Mediated Gene Targeting to Tissues *In Vivo* Following Intravenous Administration of Pegylated Immunoliposomes. *Pharm. Res.* **2001**, *18*, 1091–1095.
17. Huang, R.; Ke, W.; Liu, Y.; Jiang, C.; Pei, Y., The Use of Lactoferrin as A Ligand for Targeting the Polyamidoamine-Based Gene Delivery System to the Brain. *Biomaterials* **2008**, *29*, 238–246.
18. Liu, Y.; Huang, R.; Han, L.; Ke, W.; Shao, K.; Ye, L.; Lou, J.; Jiang, C., Brain-Targeting Gene Delivery and Cellular Internalization Mechanisms for Modified Rabies Virus Glycoprotein RVG29 Nanoparticles. *Biomaterials* **2009**, *30*, 4195–4202.
19. Zhan, C.; Li, B.; Hu, L.; Wei, X.; Feng, L.; Fu, W.; Lu, W., Micelle-Based Brain-Targeted Drug Delivery Enabled by A Nicotine Acetylcholine Receptor Ligand. *Angew. Chem. Int. Ed. Engl.* **2011**, *50*, 5482–5485.
20. He, H.; Li, Y.; Jia, X. R.; Du, J.; Ying, X.; Lu, W. L.; Lou, J. N.; Wei, Y., PEGylated Poly(amidoamine) Dendrimer-Based Dual-Targeting Carrier for Treating Brain Tumors. *Biomaterials* **2011**, *32*, 478–487.
21. Brooks, P. C.; Clark, R. A.; Cheresch, D. A., Requirement of Vascular Integrin Alpha v Beta 3 for Angiogenesis. *Science*

1
2
3 1994, 264, 569–571.

4 22. Hynes, R. O., Integrins: Bidirectional, Allosteric Signaling Machines. *Cell* **2002**, *110*, 673–687.

5 23. Schottelius, M.; Laufer, B.; Kessler, H.; Wester, H. J., Ligands for Mapping Alphavbeta3-Integrin Expression *In Vivo*.
6 *Acc. Chem. Res.* **2009**, *42*, 969–980.

7
8 24. Shibata, M.; Yamada, S.; Kumar, S. R.; Calero, M.; Bading, J.; Frangione, B.; Holtzman, D. M.; Miller, C. A.; Strickland,
9 D. K.; Ghiso, J. *et al.* Clearance of Alzheimer's Amyloid-ss(1-40) Peptide from Brain by LDL Receptor-Related Protein-1 at
10 the Blood-Brain Barrier. *J. Clin. Invest.* **2000**, *106*, 1489–1499.

11 25. Ito, S.; Ohtsuki, S.; Terasaki, T., Functional Characterization of the Brain-to-Blood Efflux Clearance of Human
12 Amyloid-Beta Peptide (1-40) across the Rat Blood-Brain Barrier. *Neurosci. Res.* **2006**, *56*, 246–252.

13 26. Demeule, M.; Regina, A.; Che, C.; Poirier, J.; Nguyen, T.; Gabathuler, R.; Castaigne, J. P.; Beliveau, R., Identification
14 and Design of Peptides as A New Drug Delivery System for the Brain. *J. Pharmacol. Exp. Ther.* **2008**, *324*, 1064–1072.

15 27. Mazza, M.; Uchegbu, I. F.; Schatzlein, A. G., Cancer and the Blood-Brain Barrier: 'Trojan Horses' for Courses? *Br. J.*
16 *Pharmacol.* **2008**, *155*, 149–151.

17 28. Maletinska, L.; Blakely, E. A.; Bjornstad, K. A.; Deen, D. F.; Knoff, L. J.; Forte, T. M., Human Glioblastoma Cell Lines:
18 Levels of Low-Density Lipoprotein Receptor and Low-Density Lipoprotein Receptor-Related Protein. *Cancer Res.* **2000**,
19 *60*, 2300–2303.

20 29. Abbott, N. J.; Patabendige, A. A.; Dolman, D. E.; Yusof, S. R.; Begley, D. J., Structure and Function of the Blood-Brain
21 Barrier. *Neurobiol. Dis.* **2010**, *37*, 13–25.

22 30. Newton, H. B., Advances in Strategies to Improve Drug Delivery to Brain Tumors. *Expert Rev Neurother* **2006**, *6*,
23 1495–1509.

24 31. Deeken, J. F.; Loscher, W., The Blood-Brain Barrier and Cancer: Transporters, Treatment, and Trojan Horses. *Clin.*
25 *Cancer Res.* **2007**, *13*, 1663–1674.

26 32. Barrett, T.; Ravizzini, G.; Choyke, P. L.; Kobayashi, H., Dendrimers in Medical Nanotechnology. *IEEE. Eng. Med. Biol.*
27 *Mag.* **2009**, *28*, 12–22.

28 33. Sarin, H.; Kanevsky, A. S.; Wu, H.; Brimacombe, K. R.; Fung, S. H.; Sousa, A. A.; Auh, S.; Wilson, C. M.; Sharma, K.;
29 Aronova, M. A. *et al.* Effective Transvascular Delivery of Nanoparticles across the Blood-Brain Tumor Barrier into
30 Malignant Glioma Cells. *J. Transl. Med.* **2008**, *6*, 80.

31 34. He, X.; Gao, J.; Gambhir, S. S.; Cheng, Z., Near-Infrared Fluorescent Nanoprobes for Cancer Molecular Imaging:
32 Status and Challenges. *Trends Mol. Med.* **2010**, *16*, 574–583.

33 35. Li, C.; Li, Y. X.; Law, G. L.; Man, K.; Wong, W. T.; Lei, H., Fast Water-Exchange Gd³⁺-(DO3A-Like) Complex
34 Functionalized with Aza-15-Crown-5 Showing Prolonged Residence Lifetime *In Vivo*. *Bioconjug. Chem.* **2006**, *17*,
35 571–574.

36 36. Yan, H.; Wang, J.; Yi, P.; Lei, H.; Zhan, C.; Xie, C.; Feng, L.; Qian, J.; Zhu, J.; Lu, W. *et al.* Imaging Brain Tumor by
37 Dendrimer-Based Optical/Paramagnetic Nanoprobe across the Blood-Brain Barrier. *Chem. Commun. (Camb)* **2011**, *47*,
38 8130–8132.

39 37. Montet, X.; Funovics, M.; Montet-Abou, K.; Weissleder, R.; Josephson, L., Multivalent Effects of RGD Peptides
40 Obtained by Nanoparticle Display. *J. Med. Chem.* **2006**, *49*, 6087–6093.

41 38. Wang, J.; Tian, S.; Petros, R. A.; Napier, M. E.; Desimone, J. M., The Complex Role of Multivalency in Nanoparticles
42 Targeting the Transferrin Receptor for Cancer Therapies. *J. Am. Chem. Soc.* **2010**, *132*, 11306–11313.

43 39. Carmeliet, P.; Jain, R. K., Angiogenesis in Cancer and Other Diseases. *Nature* **2000**, *407*, 249–257.

44 40. Choi, H. S.; Liu, W.; Misra, P.; Tanaka, E.; Zimmer, J. P.; Iitty Ipe, B.; Bawendi, M. G.; Frangioni, J. V., Renal Clearance
45 of Quantum Dots. *Nat. Biotechnol.* **2007**, *25*, 1165–1170.

46 41. Veronese, F. M.; Pasut, G., PEGylation, Successful Approach to Drug Delivery. *Drug. Discov. Today* **2005**, *10*,
47 1451–1458.

- 1
2
3 42. Li, C.; Wildes, F.; Winnard, P., Jr.; Artemov, D.; Penet, M. F.; Bhujwala, Z. M., Conjugation of Poly-L-Lysine to
4 Bacterial Cytosine Deaminase Improves the Efficacy of Enzyme/Prodrug Cancer Therapy. *J. Med. Chem.* **2008**, *51*,
5 3572–3582.
6
7 43. Wang, J.; Milner, R., Fibronectin Promotes Brain Capillary Endothelial Cell Survival and Proliferation through
8 Alpha5beta1 and Alpha5beta3 Integrins *via* MAP Kinase Signalling. *J. Neurochem.* **2006**, *96*, 148–159.
9
10 44. Veisoh, O.; Sun, C.; Fang, C.; Bhattarai, N.; Gunn, J.; Kievit, F.; Du, K.; Pullar, B.; Lee, D.; Ellenbogen, R. G. *et al.*
11 Specific Targeting of Brain Tumors with An Optical/Magnetic Resonance Imaging Nanoprobe across the Blood-Brain
12 Barrier. *Cancer Res.* **2009**, *69*, 6200–6207.
13
14 45. Corot, C.; Robert, P.; Idee, J. M.; Port, M., Recent Advances in Iron Oxide Nanocrystal Technology for Medical
15 Imaging. *Adv. Drug Deliv. Rev.* **2006**, *58*, 1471–1504.
16
17 46. Tallarida, R. J.; Raffa, R. B., The Application of Drug Dose Equivalence in the Quantitative Analysis of Receptor
18 Occupation and Drug Combinations. *Pharmacol. Ther.* **2010**, *127*, 165–174.
19
20 47. Li, C.; Winnard, P.; Bhujwala, Z. M., Facile Synthesis of 1-(Acetic
21 Acid)-4,7,10-Tris(Tert-Butoxycarbonylmethyl)-1,4,7,10-Tetraaza-Cyclododecane: A Reactive Precursor Chelating Agent.
22 *Tetrahedron Lett.* **2009**, *50*, 2929–2931.
23
24
25
26
27
28
29
30
31
32
33
34
35
36
37
38
39
40
41
42
43
44
45
46
47
48
49
50
51
52
53
54
55
56
57
58
59
60

Table of Content

